

Quantum Steering and Entanglement in a Tritter: Hierarchy under Loss

Jifeng Sun^{1,2}, Shumin Yang¹, Teng Zhao^{2,3}, Qingqian Kang^{2,4}, and Liyun Hu^{2,3*}

¹College of Electronic and Information Engineering, Nanchang Institute of Technology, Nanchang 330044, China

²Center for Quantum Science and Technology, Jiangxi Normal University, Nanchang 330022, China

³Institute for Military-Civilian Integration of Jiangxi Province, Nanchang 330200, China

⁴Department of Physics, Jiangxi Normal University Science and Technology College, Nanchang 330022, China

Multipartite entangled states of continuous variables are fundamental resources for scalable quantum information processing. We study the correlation hierarchy in a tripartite state engineered by mixing a two-mode squeezed vacuum with a coherent state on a tritter, a key linear optical element for multimode state generation. Using the covariance matrix formalism, we comprehensively analyze the entanglement and Einstein-Podolsky-Rosen (EPR) steering among the output modes. The strength of both correlations is governed solely by the squeezing parameter and is independent of the coherent amplitude. We further examine the impact of inevitable optical losses in various channel configurations. The results show that while losses degrade correlations, EPR steering remains monogamous and exhibits stricter resilience thresholds than entanglement. Our analysis, supported by parameter extension techniques, confirms that the steering condition is more stringent than the inseparability criterion, clearly demonstrating that steering forms a strict subset of entanglement. These results elucidate the correlation structure in a readily generated multimode state and offer practical insights for developing asymmetric quantum protocols, such as one-sided device-independent tasks, where EPR steering serves as a critical resource.

I. INTRODUCTION

Quantum entanglement stands as a cornerstone of quantum mechanics, epitomizing nonlocal correlations absent in classical physics [1–3]. In continuous-variable (CV) systems, Gaussian states—those with Gaussian Wigner functions—provide a fertile testbed for exploring multipartite entanglement due to their experimental accessibility and theoretical tractability [4, 5]. Beyond entanglement, Einstein-Podolsky-Rosen (EPR) steering captures a distinctive asymmetric form of quantum correlation where one party can, by local measurements, “steer” or affect the state of a distant party [6, 7]. This asymmetry grants steering unique advantages in applications such as one-sided device-independent quantum key distribution [8, 9]. The resource theory of quantum steering has been developed to quantify and understand its applications and limitations [10].

The generation of multipartite entangled states often relies on linear optical networks [11]. Among these, the tritter—a three-port balanced beam splitter—is a fundamental element for generating and manipulating three-mode Gaussian states [12]. When fed with a two-mode squeezed vacuum (TMSV) state and a coherent state, the tritter output constitutes a rich resource of tripartite quantum correlations [13]. While the hierarchy between entanglement and steering has been studied in various contexts [14, 15], a systematic analysis of this hierarchy in a tritter-generated three-mode Gaussian state, particularly under realistic loss conditions with various asymmetric configurations, remains lacking. Such an analysis is crucial for practical quantum communication where

different channels often exhibit different loss characteristics.

In this work, we fill this gap. We first derive the exact covariance matrix for the three-mode Gaussian state generated by the tritter operation on a TMSV state and a coherent state. We then employ established quantifiers based on symplectic eigenvalues to analyze bipartite and tripartite entanglement [5] and Gaussian EPR steering [14]. Our analysis reveals that the coherent state amplitude, while affecting the displacement, does not influence the strength of the quantum correlations, which are solely determined by the initial squeezing. We proceed to introduce a comprehensive model of loss, considering five distinct configurations of asymmetric and symmetric noise across the three modes. By comparing the evolution of entanglement and steering under increasing loss, we provide a concrete demonstration of the strict inclusion relation: steerable states form a proper subset of entangled states. Furthermore, we verify that the monogamy constraints of steering [15, 16] hold in all loss scenarios, underscoring the non-shareable nature of this resource. These results not only deepen the understanding of quantum correlation structures in multimode Gaussian states but also offer practical steering for designing robust quantum communication protocols in noisy environments. Specifically, our analysis of asymmetric loss configurations provides insights for optimizing resource allocation in quantum networks.

The remainder of this paper is organized as follows. In Sec. II, we introduce the tritter setup and derive the covariance matrix of the generated three-mode Gaussian state. Section III presents a detailed analysis of the entanglement and EPR steering hierarchies under ideal, lossless conditions. In Sec. IV, we model various configurations of asymmetric and symmetric loss channels and investigate their distinct impacts on both types of

* hlyun@jxnu.edu.cn

quantum correlations. We systematically compare their robustness and explicitly demonstrate the strict inclusion relation. Finally, Sec. V summarizes our main findings and discusses their implications.

II. THEORETICAL FRAMEWORK

A. The Tritter Operation and Output State

The tritter is a three-port linear optical device as shown in Fig. 1, which can be described by a unitary matrix U that transforms the input annihilation operators $\hat{a}, \hat{b}, \hat{c}$ to the output operators $\hat{a}_1, \hat{b}_1, \hat{c}_1$ [12]:

$$\begin{pmatrix} \hat{a}_1 \\ \hat{b}_1 \\ \hat{c}_1 \end{pmatrix} = U \begin{pmatrix} \hat{a} \\ \hat{b} \\ \hat{c} \end{pmatrix}, \quad \text{with } U = \frac{1}{\sqrt{3}} \begin{pmatrix} 1 & e^{2i\pi/3} & e^{2i\pi/3} \\ e^{2i\pi/3} & 1 & e^{2i\pi/3} \\ e^{2i\pi/3} & e^{2i\pi/3} & 1 \end{pmatrix}. \quad (1)$$

We consider the input state to be a product of a two-mode squeezed vacuum (TMSV) between modes a and b , and a coherent state $|\gamma\rangle_c$ in mode c :

$$|\psi_{\text{in}}\rangle = |\text{TMSV}(r)\rangle_{ab} \otimes |\gamma\rangle_c, \quad (2)$$

where $|\text{TMSV}(r)\rangle_{ab} = \frac{1}{\cosh r} \sum_{n=0}^{\infty} (\tanh r)^n |n, n\rangle_{ab}$, with $r \geq 0$ being the squeezing parameter, and $|\gamma\rangle_c = e^{\gamma\hat{c}^\dagger - \gamma^* \hat{c}} |0\rangle_c$.

The squeezing operator is defined as $\hat{S}(r) = \exp[r(\hat{a}\hat{b} - \hat{a}^\dagger\hat{b}^\dagger)]$, and the displacement operator as $\hat{D}_c(\gamma) = \exp(\gamma\hat{c}^\dagger - \gamma^* \hat{c})$. The explicit form of the output state after the tritter operation can be expressed as:

$$|\psi_{\text{out}}\rangle = \frac{1}{\cosh r} \exp\left(-\frac{|\gamma|^2}{2} + \hat{O}_{T1} + \hat{O}_{T2}\right) |000\rangle_{abc}, \quad (3)$$

where $\hat{O}_{T1} = \frac{\lambda}{3} \left[e^{-2i\pi/3} (\hat{a}^{\dagger 2} + \hat{b}^{\dagger 2}) + e^{2i\pi/3} \hat{c}^{\dagger 2} + e^{i\pi/3} \hat{a}^\dagger \hat{b}^\dagger \right]$ and $\hat{O}_{T2} = \frac{\gamma}{\sqrt{3}} \left[e^{-2i\pi/3} (\hat{a}^\dagger + \hat{b}^\dagger) - \hat{b}^\dagger \hat{c}^\dagger - \hat{a}^\dagger \hat{c}^\dagger \right]$, with $\lambda = \tanh r$.

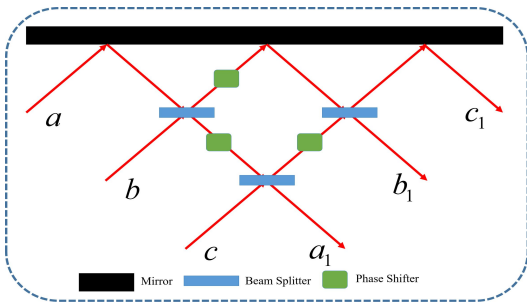


FIG. 1. Schematic diagram of a three-mode optical splitter (Tritter). The blue components represent beam splitters, the green components represent phase shifters, and the black components represent mirrors.

B. Covariance Matrix Formalism

For Gaussian states, all information about quantum correlations is contained in the first and second statistical moments. Since displacements do not affect entanglement or steering measures for Gaussian states, we focus on the covariance matrix (CM) \mathbf{V} . For a three-mode system with quadrature vector $\xi = (\hat{x}_a, \hat{p}_a, \hat{x}_b, \hat{p}_b, \hat{x}_c, \hat{p}_c)^\top$, the CM elements are $V_{ij} = \frac{1}{2} \langle \{\Delta\hat{\xi}_i, \Delta\hat{\xi}_j\} \rangle$, where $\Delta\hat{\xi}_i = \hat{\xi}_i - \langle \hat{\xi}_i \rangle$.

The CM of the output state $|\psi_{\text{out}}\rangle$ is derived analytically (see Appendix):

$$\mathbf{V} = \frac{\mathbf{I}_6}{2} + \frac{1}{1 - \lambda^2} \begin{pmatrix} \mathbf{V}_{11} & \mathbf{V}_{12} & \mathbf{V}_{13} \\ \mathbf{V}_{12}^\top & \mathbf{V}_{22} & \mathbf{V}_{23} \\ \mathbf{V}_{13}^\top & \mathbf{V}_{23}^\top & \mathbf{V}_{33} \end{pmatrix}, \quad (4)$$

where $\lambda = \tanh r$, and the 2×2 submatrices \mathbf{V}_{ij} are given by:

$$\mathbf{V}_{11} = \mathbf{V}_{22} = \mathbf{V}_{33} = \frac{\lambda}{3} \begin{pmatrix} 2\lambda - 1 & -\sqrt{3} \\ -\sqrt{3} & 2\lambda + 1 \end{pmatrix}, \quad (5)$$

$$\mathbf{V}_{12} = \frac{\lambda}{6} \begin{pmatrix} 1 - 2\lambda & \sqrt{3} \\ \sqrt{3} & -1 - 2\lambda \end{pmatrix}, \quad (6)$$

$$\mathbf{V}_{13} = \mathbf{V}_{23} = \frac{\lambda}{6} \begin{pmatrix} \lambda - 2 & -\sqrt{3}\lambda \\ \sqrt{3}\lambda & \lambda + 2 \end{pmatrix}. \quad (7)$$

Crucially, the CM is independent of γ , confirming that displacement does not alter the correlation structure.

C. Quantifiers for Entanglement and Steering

For a bipartite split of a Gaussian state with CM \mathbf{V}_{AB} , entanglement can be detected via the positive partial transpose (PPT) criterion [17, 18]. The logarithmic negativity $E^{A|B}$ quantifies entanglement [5]:

$$E^{A|B} = \max \left[0, - \sum_{j: \nu_j^{AB^\top} < 1/2} \ln(2\nu_j^{AB^\top}) \right], \quad (8)$$

where $\{\nu_j^{AB^\top}\}$ are the symplectic eigenvalues of the partially transposed CM.

Gaussian EPR steering from party A to party B is quantified by [14]:

$$S^{A \rightarrow B} = \max \left[0, - \sum_{j: \bar{\nu}_j^{B|A} < 1/2} \ln(2\bar{\nu}_j^{B|A}) \right], \quad (9)$$

where $\{\bar{\nu}_j^{B|A}\}$ are the symplectic eigenvalues of the Schur complement $\mathbf{V}^{B|A} = \mathbf{V}_B - \mathbf{V}_C^\top \mathbf{V}_A^{-1} \mathbf{V}_C$, with \mathbf{V}_{AB} partitioned as:

$$\mathbf{V}_{AB} = \begin{pmatrix} \mathbf{V}_A & \mathbf{V}_C \\ \mathbf{V}_C^\top & \mathbf{V}_B \end{pmatrix}. \quad (10)$$

A nonzero value indicates steerability from A to B . The measure is asymmetric: $S^{A \rightarrow B} \neq S^{B \rightarrow A}$ in general.

III. QUANTUM CORRELATIONS UNDER IDEAL CONDITIONS

A. Entanglement Structure

Using Eq. (8), we compute the bipartite entanglement for all possible splits. For any two modes i and j ($i, j \in \{a, b, c\}$), the bipartite entanglement is:

$$E^{i|j} = \ln \left[\frac{3(1+\lambda)}{3-\lambda} \right]. \quad (11)$$

For the split between one mode k and the remaining two modes ij , the tripartite entanglement is:

$$E^{k|ij} = \ln \left[\frac{9(1-\lambda^2)}{(\sqrt{9-\lambda^2} - \sqrt{8}\lambda)^2} \right]. \quad (12)$$

Both measures are positive for $\lambda > 0$ and increase monotonically with λ , as shown in Fig. 2. Moreover, $E^{k|ij} > E^{i|j}$ for all $\lambda > 0$, indicating stronger entanglement in the 1 vs 2 partition. The nonzero entanglement across all bipartitions confirms that the output state is a genuinely tripartite entangled Gaussian state.

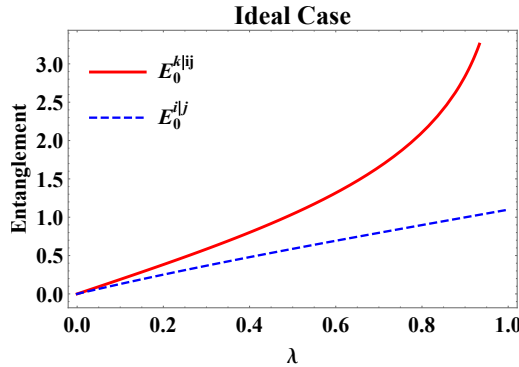


FIG. 2. Evolution of entanglement with squeezing parameter λ . Blue dashed line: tripartite entanglement $E^{k|ij}$; red dotted line: bipartite entanglement $E^{i|j}$.

B. EPR Steering Hierarchy

Applying Eq. (9), we find a starkly different structure for steering. The steering measures between any two individual modes vanish identically:

$$S^{i \leftrightarrow j} = 0, \quad \forall i, j. \quad (13)$$

However, steering exists between a single mode and the group of the other two:

$$S^{k \rightarrow ij} = S^{ij \rightarrow k} = \ln \left[\frac{9 - \lambda^2}{9(1 - \lambda^2)} \right] > 0 \quad \text{for } \lambda > 0. \quad (14)$$

This demonstrates a strict hierarchy: while all modes are pairwise entangled, no pairwise steering exists. Steering

is only present in the collective 1 vs 2 partition, and it is *symmetric* ($S^{k \rightarrow ij} = S^{ij \rightarrow k}$) in the ideal case.

The monogamy of Gaussian steering [15, 16] imposes constraints:

$$S^{ij \rightarrow k} - S^{i \rightarrow k} - S^{j \rightarrow k} \geq 0, \quad S^{k \rightarrow ij} - S^{k \rightarrow i} - S^{k \rightarrow j} \geq 0. \quad (15)$$

Given $S^{i \rightarrow k} = S^{k \rightarrow i} = 0$, these inequalities are trivially satisfied, indicating no sharing of steering exists in the ideal output state.

C. Physical Mechanism and Interpretation

Ideal conditions reveal the phenomenon of "entanglement without steering" between any two modes, which has profound physical origins. Although squeezing creates quantum entanglement between modes, the symmetric operation of the tritter evenly distributes correlations, resulting in insufficient asymmetry between any two modes to support steering. This symmetry breaking is a common phenomenon in linear optical networks, analogous to photon bunching in Hong-Ou-Mandel interference.

From a phase-space perspective, the tritter's unitary transformation (Eq. 1) mixes the quadratures of all three modes symmetrically. This symmetric mixing dilutes any directional dependence in the correlations, making it impossible for one mode to unilaterally determine the state of another. The preservation of entanglement, however, indicates that non-classical correlations remain, albeit in a symmetric form that cannot be exploited for steering.

From a resource theory perspective [10], steering requires not only non-classical correlations but also sufficient control of one party over the state of another. In the three-mode system, despite entanglement between any two modes, the involvement of the third mode prevents any single party from completely determining the state of another—a direct manifestation of correlation sharing and resource competition in multipartite systems. Our calculations align with the monogamy constraints of multipartite steering [15, 16] and provide quantitative tools for understanding correlation distribution in multipartite systems.

IV. ROBUSTNESS AGAINST LOSS

A. Loss Model

To model realistic conditions, we incorporate loss channels in each output mode of the tritter, as depicted in Fig. 3. Each channel is characterized by a transmissivity $T_i = \cos^2 \theta_i$ ($i = 1, 2, 3$), with $T_i = 1$ representing no loss. The effect on the CM is a simple scaling: the CM V^{lossy} is obtained from the ideal CM V [Eq. (4)] by the transformation $V_{ij} \rightarrow \sqrt{T_i T_j} V_{ij}$ for $i \neq j$, and $V_{ii} \rightarrow T_i V_{ii} + (1 - T_i) I_2 / 2$.

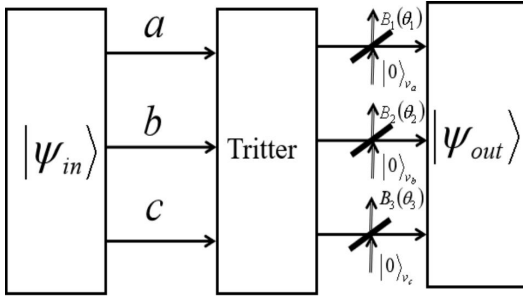


FIG. 3. The model describing how the input state undergoes Tritter processing to produce the output state under noise influence.

We analyze five representative loss configurations (Scenarios 1–5) to understand the effect of asymmetric versus symmetric loss on the correlation hierarchy [19, 20]. These scenarios are defined as follows:

- **Scenario 1: Single-mode loss** - Only mode k experiences loss, $T_i = T_j = 1, T_k = T$.
- **Scenario 2: Loss at one mode of the pair** - Only one mode in the dual-mode module experiences loss, $T_i = T, T_j = T_k = 1$ or $T_j = T, T_i = T_k = 1$.
- **Scenario 3: Group-matched dual-mode loss** - Both modes in the dual-mode module experience loss, $T_i = T_j = T, T_k = 1$.
- **Scenario 4: Intergroup dual-mode loss** - One mode in the pair and mode k experience loss, $T_i = T_k = T, T_j = 1$ or $T_j = T_k = T, T_i = 1$.
- **Scenario 5: Triple-mode loss** - All three modes experience loss, $T_i = T_j = T_k = T$.

B. Evolution of Quantum Correlations under Loss

1. Entanglement

Based on the entanglement metric defined in Eq. (8), the bipartite entanglement under loss is given by:

$$E_1^{i|j} = \ln \left[\frac{9(1 - \lambda^2)}{9 - \delta_1 \lambda^2 - 4\lambda\sqrt{\delta_2 \lambda^2 + 9T}} \right], \quad (16)$$

$$E_2^{i|j} = \ln \left[\frac{3(1 - \lambda^2)}{(3 - 3\lambda + 2T\lambda)(1 + \lambda + 2T\lambda)} \right], \quad (17)$$

where $\delta_1 = 5 - 16T + 8T^2$, $\delta_2 = (1 - T)^2(1 - 8T + 4T^2)$. Subscript 1 indicates loss in one of the two modes, while subscript 2 indicates loss in both modes.

For tripartite entanglement $E^{k|ij}$, analytical expres-

sions for Scenarios 1, 3, and 5 are:

$$E_1^{k|ij} = \ln \left[\frac{9(1 - \lambda^2)}{9 - \epsilon_1 \lambda^2 - 4\lambda\sqrt{18T + \epsilon_2 \lambda^2}} \right], \quad (18)$$

$$E_3^{k|ij} = \ln \left[\frac{9(1 - \lambda^2)}{9 - \epsilon_3 \lambda^2 - 2\lambda\sqrt{72T + \epsilon_4 \lambda^2}} \right], \quad (19)$$

$$E_5^{k|ij} = \ln \left[\frac{9(1 - \lambda^2)}{9 - \epsilon_5 \lambda^2 - 2T\lambda\sqrt{72 + \epsilon_6 \lambda^2}} \right], \quad (20)$$

where $\epsilon_1 = 5 - 20T + 8T^2$, $\epsilon_2 = (1 - 4T + T^2)(1 - 2T)^2$, $\epsilon_3 = 5 - 14T + 2T^2$, $\epsilon_4 = (1 - 10T + T^2)(2 - T)^2$, $\epsilon_5 = 9 - 18T + 2T^2$, $\epsilon_6 = 9 - 18T + T^2$.

For completeness, we provide the tripartite entanglement expressions for Scenarios 2 and 4, which are more complex but can be derived using the same methodology. For Scenario 2 (loss in one mode of the pair, say $T_i = T, T_j = T_k = 1$), we have:

$$E_2^{k|ij} = \ln \left[\frac{9(1 - \lambda^2)}{9 - \zeta_1 \lambda^2 - 2\lambda\sqrt{36T + \zeta_2 \lambda^2}} \right], \quad (21)$$

where $\zeta_1 = 5 - 12T + 4T^2$, $\zeta_2 = (1 - 2T)^2(1 - 4T + T^2)$.

$$E_4^{k|ij} = \ln \left[\frac{9(1 - \lambda^2)}{9 - \eta_1 \lambda^2 - 2\lambda\sqrt{36T + \eta_2 \lambda^2 + \eta_3 T^2}} \right], \quad (22)$$

where $\eta_1 = 5 - 16T + 8T^2$, $\eta_2 = (1 - 4T + T^2)^2$, $\eta_3 = 8T(1 - T)^2$.

Both bipartite $E^{i|j}$ and tripartite $E^{k|ij}$ entanglement decrease monotonically with increasing loss (decreasing T), as shown in Figs. 4 and 5. For bipartite entanglement, it is more fragile when loss affects both modes involved in the partition. Furthermore, the rate of entanglement decay under loss increases with the squeezing parameter λ . Bipartite entanglement abruptly vanishes under significant loss when λ exceeds a certain threshold. The underlying physical mechanism is that a larger squeezing parameter λ corresponds to a higher average photon number, which enhances the interaction between the light field and the lossy environment, making entanglement more sensitive to loss.

To clarify the impact of loss distribution on the tripartite entanglement of the output state, we compare the entanglement evolution curves as a function of reflectivity in the five scenarios, as shown in Fig. 6. The figure reveals significant differences in entanglement strength across the various loss distributions, ranked from strongest to weakest as follows: $E_2^{k|ij} > E_3^{k|ij} > E_1^{k|ij} > E_4^{k|ij} > E_5^{k|ij}$.

2. Steering

The steerability $S^{i \rightarrow j}$ between any two modes i and j can be calculated using the symplectic eigenvalues $v^{j|i}$

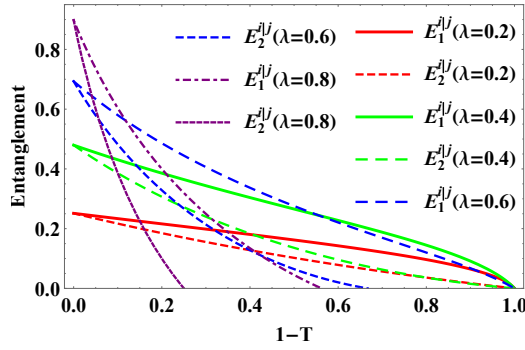


FIG. 4. Bipartite entanglement $E^{i|j}$ versus reflectivity $(1 - T)$ for different squeezing parameters λ .

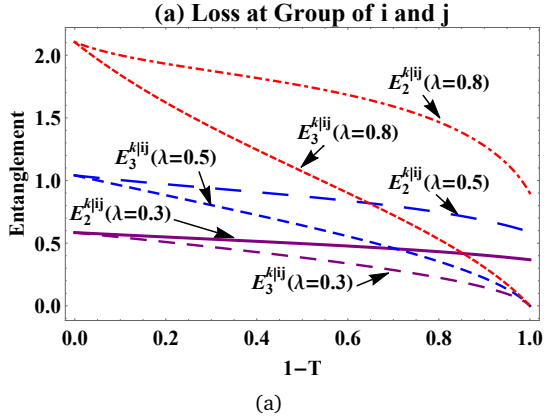


FIG. 5. Curves of tripartite entanglement versus reflectivity under different noise loss conditions. (a) Two cases with no loss in mode k , (b) Three cases with loss in mode k .

of the Schur complement $V^{j|i}$. In the loss model, the corresponding symplectic eigenvalues can be expressed as:

$$v_1^{j|i} = v_2^{j|i} = \sqrt{\frac{9 - 2\xi_1\lambda^2 + \xi_2^2\lambda^4}{4(1 - \lambda^2)[9 - (3 - T_i)^2\lambda^2]}}, \quad (23)$$

where $\xi_1 = 9 + 8(T_i^2 + T_j^2) - 12(T_i + T_j) + 4T_iT_j$, $\xi_2 = 3 - 4(T_i + T_j - T_iT_j)$. Since $v_1^{j|i} = v_2^{j|i} \geq \frac{1}{2}$, ac-

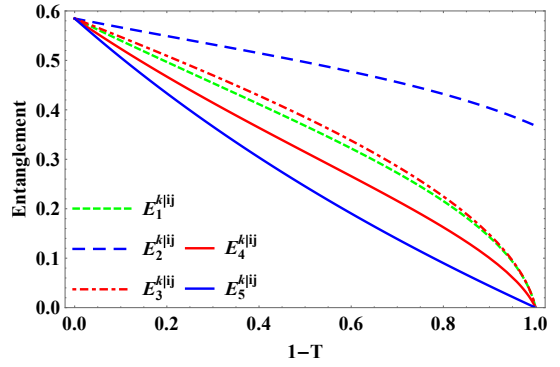


FIG. 6. Comparison of tripartite entanglement $E^{k|ij}$ versus reflectivity under different loss configurations for (a) $\lambda = 0.3$, (b) $\lambda = 0.8$.

cording to the definition of the steering metric in Eq. (9), no quantum steering relationship exists between any two modes. Thus, the system satisfies the steering monogamy relation under loss.

Similarly, tripartite steering in the five scenarios is given by:

Scenario 1:

$$S_1^{ij \rightarrow k} = \ln \left[\frac{9 - \lambda^2}{9 - (1 - 4T)^2\lambda^2} \right], \quad (24)$$

$$S_1^{k \rightarrow ij} = \ln \left[\frac{9 - (3 - 4T)^2\lambda^2}{9 - (1 - 4T)^2\lambda^2} \right]. \quad (25)$$

Scenario 2:

$$S_2^{ij \rightarrow k} = \ln \left[\frac{9 - 2(5 - 8T + 8T^2)\lambda^2 + \lambda^4}{(1 - \lambda^2)[9 - (1 - 4T)^2\lambda^2]} \right], \quad (26)$$

$$S_2^{k \rightarrow ij} = \ln \left[\frac{(1 - \lambda^2)(9 - \lambda^2)}{(1 - \lambda^2)(9 - \lambda^2) + \chi_1 - 4\lambda^2\sqrt{T\chi_2}} \right], \quad (27)$$

where $\chi_1 = 4T\lambda^2(1 + \lambda^2 - 2T)$, $\chi_2 = (1 - \lambda^2)(9 - \lambda^2) + 4T^3 - 4T^2(1 + \lambda^2) - 4T(2 - 3\lambda^2)$.

Scenario 3:

$$S_3^{ij \rightarrow k} = \ln \left[\frac{9 - (3 - 2T)^2 \lambda^2}{9 - (1 + 2T)^2 \lambda^2} \right], \quad (28)$$

$$S_3^{k \rightarrow ij} = \ln \left[\frac{9 - \lambda^2}{9 - (1 + 2T)^2 \lambda^2} \right]. \quad (29)$$

Scenario 4:

$$S_4^{ij \rightarrow k} = \ln \left[\frac{9 - 2(5 - 8T + 8T^2) \lambda^2 + \lambda^4}{9 - 2(5 - 16T + 20T^2) \lambda^2 + (1 - 4T^2)^2 \lambda^4} \right], \quad (30)$$

$$S_4^{k \rightarrow ij} = \ln \left[\frac{(1 - \lambda^2)[9 - (3 - 4T)^2 \lambda^2]}{9 + \vartheta_0 \lambda^4 - 2\lambda^2 [\vartheta_1 + 2\sqrt{\vartheta_2 + \vartheta_3 + \vartheta_4 + \vartheta_5}]} \right], \quad (31)$$

with $\vartheta_0 = 5 - 50T + 28T^2 + 16T^3 + 8T^4$, $\vartheta_1 = 7 - 14T + 14T^2$, $\vartheta_2 = 4T^8 \lambda^4 - 16T^7 \lambda^4$, $\vartheta_3 = (1 - \lambda^2)^2 - 4T^6 \lambda^2 (3 - 7\lambda^2) + T^5 \lambda^2 (60 - 52\lambda^2)$, $\vartheta_4 = T(-7 + 18\lambda^2 - 11\lambda^4) - 4T^3(6 - 29\lambda^2 + 23\lambda^4)$, $\vartheta_5 = T^2(22 - 64\lambda^2 + 46\lambda^4) + T^4(9 - 118\lambda^2 + 93\lambda^4)$.

Scenario 5:

$$S_5^{ij \rightarrow k} = \ln \left[\frac{9 - (3 - 2T)^2 \lambda^2}{9 - (3 - 6T)^2 \lambda^2} \right], \quad (32)$$

$$S_5^{k \rightarrow ij} = \ln \left[\frac{9 - (3 - 4T)^2 \lambda^2}{9 - (3 - 6T)^2 \lambda^2} \right]. \quad (33)$$

According to Eqs. (26)–(35), we can derive the conditions for steering in the five scenarios:

$$S_1^{ij \rightarrow k} > 0 : T > 0.5, \quad S_1^{k \rightarrow ij} > 0 : T > 0.5, \quad (34)$$

$$S_2^{ij \rightarrow k} > 0 : 0 < T \leq 1, \quad S_2^{k \rightarrow ij} > 0 : 0 < T \leq 1, \quad (35)$$

$$S_3^{ij \rightarrow k} > 0 : T > 0.5, \quad S_3^{k \rightarrow ij} > 0 : 0 < T \leq 1, \quad (36)$$

$$S_4^{ij \rightarrow k} > 0 : T > 2/3, \quad S_4^{k \rightarrow ij} > 0 : T > 0.5, \quad (37)$$

$$S_5^{ij \rightarrow k} > 0 : T > 3/4, \quad S_5^{k \rightarrow ij} > 0 : T > 3/5. \quad (38)$$

Tripartite steering exhibits a more nuanced and stricter behavior. The symmetric steering $S^{k \rightarrow ij} = S^{ij \rightarrow k}$ present in the ideal case is broken by loss, leading to directional asymmetry. More critically, steering vanishes at finite transmissivity thresholds, which depend on the loss configuration. Fig. 7 plots the steering measures versus loss for different scenarios. Key observations:

- Steering from a single mode to the other two modes is more robust than the reverse direction.
- The thresholds for $S^{ij \rightarrow k} > 0$ are generally stricter than for $S^{k \rightarrow ij} > 0$.
- In Scenario 2 (loss only in one of modes i and j), steering persists for all $T > 0$, demonstrating the highest robustness.
- In Scenario 5 (symmetric loss in all modes), steering vanishes at the highest thresholds.

To investigate the influence of loss distributions on steering, we plot the steering curve as a function of reflectivity $1 - T$ in Fig. 8. The results reveal significant differences in steering intensity across the five scenarios, ranked from strongest to weakest as follows: Scenario 2, Scenario 3, Scenario 1, Scenario 4, and Scenario 5.

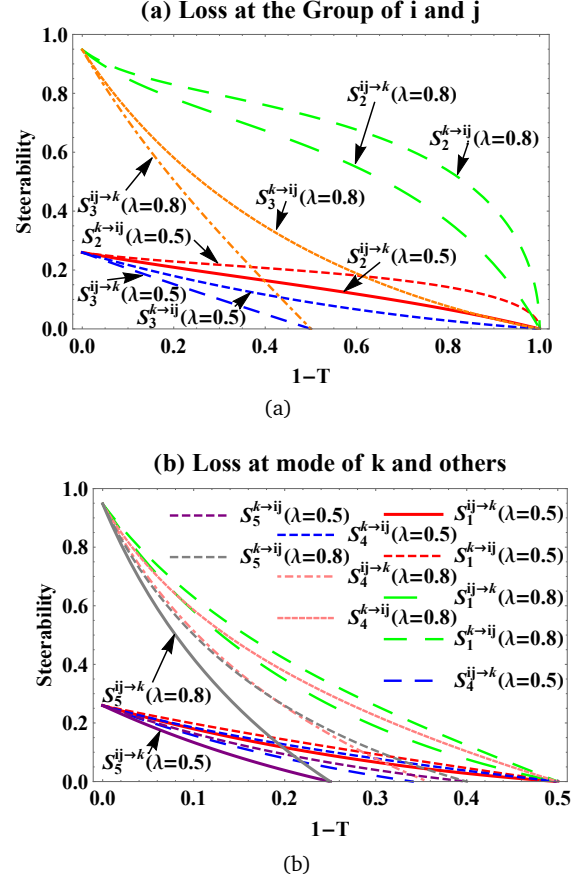


FIG. 7. Steering versus reflectivity under different loss configurations. (a) Two cases with lossless single-mode modules; (b) Three cases with lossy single-mode modules.

C. Physical Significance of Loss Asymmetry

The differences in correlation behavior under various loss configurations reveal the sensitivity of quantum resources to environmental noise and its intrinsic connection to system structure. When loss affects only a single mode (Scenario 1) or one mode in a pair (Scenario 2), the system retains sufficient asymmetry to preserve steering in certain directions. This is highly relevant to practical applications in one-sided device-independent protocols, where different channels in real quantum communication often have different transmission efficiencies [9].

Interestingly, the highest robustness of steering in Scenario 2 (loss in only one mode of the dual-mode compo-

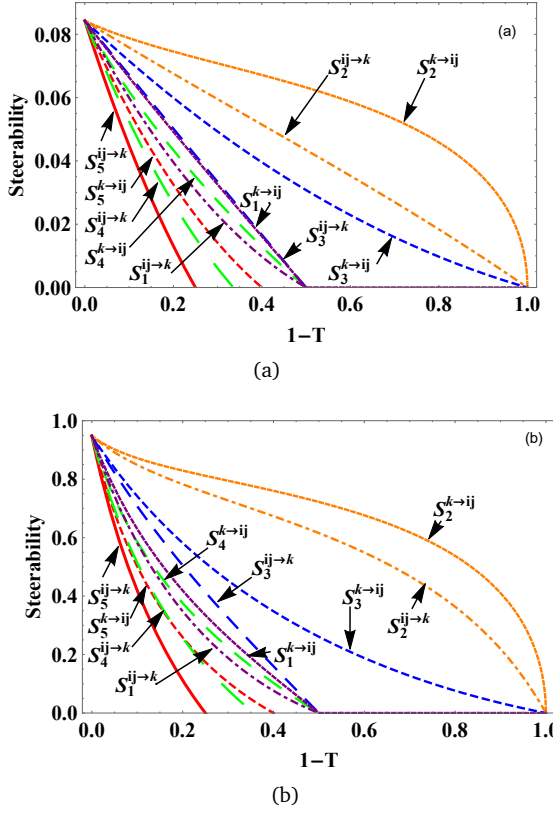


FIG. 8. Steering versus reflectivity under different loss modes. (a) $\lambda = 0.3$; (b) $\lambda = 0.8$.

nent) suggests the effectiveness of a "partial protection" strategy: by selectively protecting key connections within the system, specific quantum resources can be maximally maintained. For instance, in a quantum network where nodes are connected via lossy channels, prioritizing the protection of certain channels (e.g., those with lower intrinsic loss or those that carry critical steering resources) can help maintain asymmetric quantum correlations needed for tasks like one-sided device-independent quantum key distribution. This finding provides new insights for designing fault-tolerant quantum networks [20].

D. Correlation Hierarchy and Operational Distinction

The differential decay of entanglement and steering under loss provides a clear operational demarcation within the quantum correlation hierarchy. As shown in Figs. 9–13, for a fixed λ , as loss increases, the following sequence occurs:

1. **Region I (Low loss):** Both steering and entanglement are present.
2. **Region II (Moderate loss):** Steering disappears (first $S^{ij \rightarrow k}$, then possibly $S^{k \rightarrow ij}$), while entanglement remains.

3. **Region III (High loss):** Only entanglement remains until it too eventually vanishes for extremely high loss.

This confirms that the set of steerable states is a strict subset of the set of entangled states for the tritter-generated state under loss. The monogamy constraints [Eq. (15)] continue to hold in all lossy scenarios, as verified by our calculations.

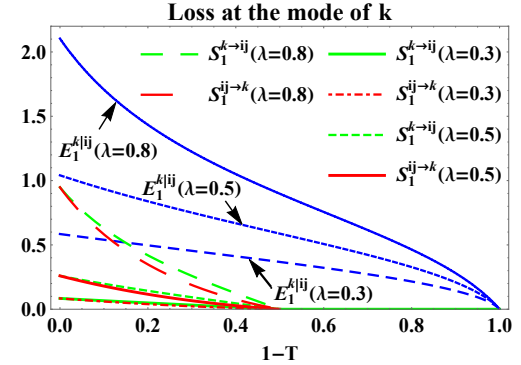


FIG. 9. Steering and entanglement evolution in Scenario 1.

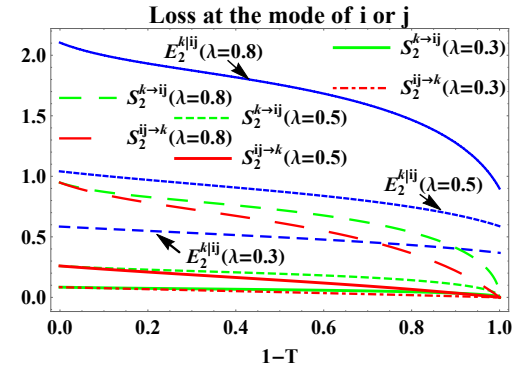


FIG. 10. Steering and entanglement evolution in Scenario 2.

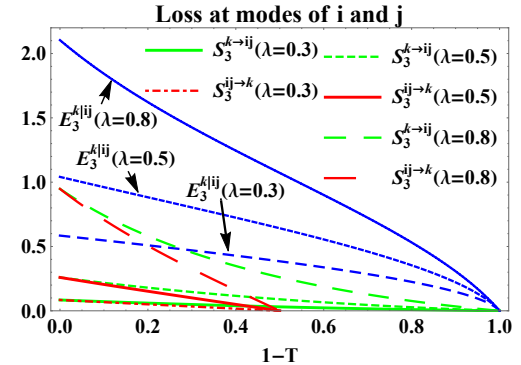


FIG. 11. Steering and entanglement evolution in Scenario 3.

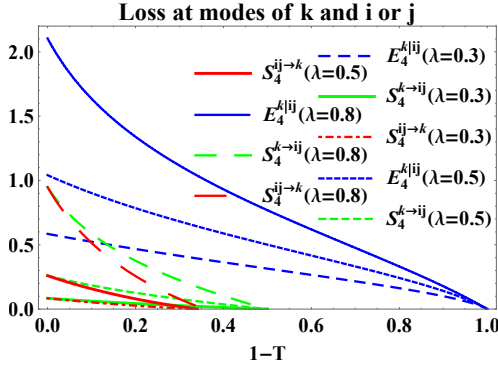


FIG. 12. Steering and entanglement evolution in Scenario 4.

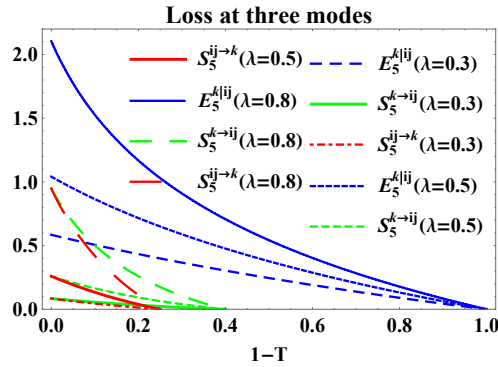


FIG. 13. Steering and entanglement evolution in Scenario 5.

E. Revisiting the Hierarchy between Steering and Entanglement

Our results clearly demonstrate the strict hierarchy of quantum correlations: steering \subset entanglement. This relationship is evident not only in existence but also in robustness—entanglement persists at higher noise levels. This difference stems from the distinct operational definitions of the two resources: entanglement only requires non-classical correlations, while steering further requires causal influence of one party over the state of another [6, 10].

From a practical perspective, this hierarchical relationship provides multiple layers of security for quantum protocols. In low-noise environments, both entanglement and steering can be leveraged to provide stronger security guarantees; in high-noise environments, even if steering disappears, entanglement can still support basic quantum communication tasks. Our tritter system provides a clear and controllable experimental platform for this purpose, complementing recent experimental demonstrations of continuous-variable steering in tripartite systems [21].

V. CONCLUSION

We have performed a detailed analytical study of the hierarchy of quantum correlations in a three-mode Gaussian state generated by a tritter acting on a TMSV state and a coherent state. The ideal output state exhibits genuine tripartite entanglement and symmetric collective steering (1 vs 2 modes) but no bipartite steering, establishing a clear correlation structure.

Under realistic loss, entanglement proves more robust than steering, with the latter vanishing at finite transmissivity thresholds that depend on the loss distribution. This provides a concrete, experimentally relevant example where steering is a stricter resource than entanglement. The monogamy of steering remains intact, preserving its non-shareable character.

Our results offer valuable insights for designing quantum information protocols that rely on different grades of quantum correlations. The tritter setup provides a versatile platform for generating states with tailored correlation properties, where EPR steering—a critical resource for one-sided device-independent tasks—can be selectively maintained or degraded by controlling loss asymmetry. Future work may explore experimental realizations of these correlations using integrated photonic triters, dynamics in non-Markovian environments, or applications in multi-user quantum network primitives. Experimental demonstrations of continuous-variable steering in tripartite systems [21] and further development of resource theories [10] will also be important for advancing practical applications.

ACKNOWLEDGMENTS

This work is supported by the National Natural Science Foundation of China (Grants No. 12564049 and No. 12104195), the Jiangxi Provincial Natural Science Foundation (Grants No. 20242BAB26009 and 20232BAB211033), the Jiangxi Provincial Key Laboratory of Advanced Electronic Materials and Devices (Grant No. 2024SSY03011), and the Jiangxi Civil-Military Integration Research Institute (Grant No. 2024JXRH0Y07).

Appendix A: Derivation of the Covariance Matrix

The characteristic function formalism provides an efficient way to compute moments. The Wigner characteristic function for the output state $|\psi_{\text{out}}\rangle$ is defined as $\chi_W(\xi) = \langle\psi_{\text{out}}|\hat{D}(\xi)|\psi_{\text{out}}\rangle$, where $\hat{D}(\xi) = \exp(i\xi^\top \Omega \hat{R})$ is the displacement operator, $\hat{R} = (\hat{x}_a, \hat{p}_a, \dots)^\top$, and $\Omega = \bigoplus_{i=1}^3 \begin{pmatrix} 0 & 1 \\ -1 & 0 \end{pmatrix}$ is the symplectic form.

According to the characteristic function theory, the relationship between the normally ordered characteristic function and the Wigner characteristic function is

$\chi_N(\xi) = e^{|\xi|^2/2} \chi_W(\xi)$. The characteristic function of the output state can be expressed as:

$$\chi_W(\xi) = \exp \left[-\frac{1}{2} \xi^\top (\mathbf{V} + \frac{1}{2} \mathbf{I}) \xi + i \xi^\top \boldsymbol{\Omega} \langle \hat{\mathbf{R}} \rangle \right], \quad (\text{A1})$$

where \mathbf{V} is the covariance matrix and $\langle \hat{\mathbf{R}} \rangle$ is the first moment vector.

The normally ordered characteristic function $\chi_N(\xi) = \langle \psi_{\text{out}} | e^{\xi^\top \hat{\mathbf{a}}^\dagger} e^{-\xi^\top \hat{\mathbf{a}}} | \psi_{\text{out}} \rangle$ is related to χ_W by $\chi_N(\xi) = e^{\frac{1}{2} |\xi|^2} \chi_W(\xi)$, where $\hat{\mathbf{a}} = (\hat{a}, \hat{b}, \hat{c})^\top$. The first and second moments can then be obtained via derivatives:

$$\langle \hat{R}_i \rangle = \frac{\partial \chi_N(\xi)}{\partial \xi_i} \Big|_{\xi=0}, \quad \langle \hat{R}_i \hat{R}_j \rangle = \frac{\partial^2 \chi_N(\xi)}{\partial \xi_i \partial \xi_j} \Big|_{\xi=0}. \quad (\text{A2})$$

Applying this procedure to the state generated by Eqs. (2) and (1) yields the CM in Eq. (4) and the first moments $\langle \hat{\mathbf{R}} \rangle$, which depend linearly on γ but do not affect the CM.

From Eq. (A2), the covariance matrix elements of the output state are calculated as follows:

$$C(\hat{x}_i, \hat{x}_i) = \frac{3 - 2\lambda + \lambda^2}{6(1 - \lambda^2)} \quad (i = a, b, c), \quad (\text{A3})$$

$$C(\hat{p}_i, \hat{p}_i) = \frac{3 + 2\lambda + \lambda^2}{6(1 - \lambda^2)} \quad (i = a, b, c), \quad (\text{A4})$$

$$C(\hat{x}_i, \hat{p}_i) = C(\hat{p}_i, \hat{x}_i) = -\frac{\sqrt{3}\lambda}{3(1 - \lambda^2)} \quad (i = a, b), \quad (\text{A5})$$

$$C(\hat{x}_c, \hat{p}_c) = C(\hat{p}_c, \hat{x}_c) = \frac{\sqrt{3}\lambda}{3(1 - \lambda^2)}, \quad (\text{A6})$$

$$C(\hat{p}_a, \hat{x}_c) = C(\hat{x}_c, \hat{p}_a) = \frac{\sqrt{3}\lambda^2}{6(1 - \lambda^2)}, \quad (\text{A7})$$

$$C(\hat{p}_b, \hat{x}_c) = C(\hat{x}_c, \hat{p}_b) = \frac{\sqrt{3}\lambda^2}{6(1 - \lambda^2)}, \quad (\text{A8})$$

$$C(\hat{x}_b, \hat{p}_c) = C(\hat{p}_c, \hat{x}_b) = -\frac{\sqrt{3}\lambda^2}{6(1 - \lambda^2)}, \quad (\text{A9})$$

$$C(\hat{p}_c, \hat{x}_a) = C(\hat{x}_a, \hat{p}_c) = -\frac{\sqrt{3}\lambda^2}{6(1 - \lambda^2)}, \quad (\text{A10})$$

$$C(\hat{p}_b, \hat{p}_c) = C(\hat{p}_c, \hat{p}_b) = \frac{\lambda(\lambda + 2)}{6(1 - \lambda^2)}, \quad (\text{A11})$$

$$C(\hat{p}_c, \hat{p}_a) = C(\hat{p}_a, \hat{p}_c) = \frac{\lambda(\lambda + 2)}{6(1 - \lambda^2)}, \quad (\text{A12})$$

$$C(\hat{x}_b, \hat{x}_c) = C(\hat{x}_c, \hat{x}_b) = \frac{\lambda(\lambda - 2)}{6(1 - \lambda^2)}, \quad (\text{A13})$$

$$C(\hat{x}_c, \hat{x}_a) = C(\hat{x}_a, \hat{x}_c) = \frac{\lambda(\lambda - 2)}{6(1 - \lambda^2)}, \quad (\text{A14})$$

$$C(\hat{p}_a, \hat{p}_b) = C(\hat{p}_b, \hat{p}_a) = -\frac{\lambda(1 + 2\lambda)}{6(1 - \lambda^2)}, \quad (\text{A15})$$

$$C(\hat{x}_a, \hat{x}_b) = C(\hat{x}_b, \hat{x}_a) = \frac{\lambda(1 - 2\lambda)}{6(1 - \lambda^2)}, \quad (\text{A16})$$

$$C(\hat{x}_a, \hat{p}_b) = C(\hat{p}_b, \hat{x}_a) = \frac{\sqrt{3}\lambda}{6(1 - \lambda^2)}, \quad (\text{A17})$$

$$C(\hat{x}_b, \hat{p}_a) = C(\hat{p}_a, \hat{x}_b) = \frac{\sqrt{3}\lambda}{6(1 - \lambda^2)}. \quad (\text{A18})$$

[1] A. Einstein, B. Podolsky, and N. Rosen, Phys. Rev. **47**, 777 (1935).
[2] E. Schrödinger, Math. Proc. Cambridge Philos. Soc. **31**, 555 (1935).
[3] E. Schrödinger, Math. Proc. Cambridge Philos. Soc. **32**, 446 (1936).
[4] C. Weedbrook et al., Rev. Mod. Phys. **84**, 621 (2012).
[5] G. Adesso and F. Illuminati, J. Phys. A: Math. Theor. **40**, 7821 (2007).
[6] H. M. Wiseman, S. J. Jones, and A. C. Doherty, Phys. Rev. Lett. **98**, 140402 (2007).
[7] S. J. Jones, H. M. Wiseman, and A. C. Doherty, Phys. Rev. A **76**, 052116 (2007).
[8] C. Branciard, E. G. Cavalcanti, S. P. Walborn, V. Scarani, and H. M. Wiseman, Phys. Rev. A **85**, 010301 (2012).
[9] S.-L. Zhou, Y.-B. Sheng, and L. Zhou, Phys. Rev. Applied **14**, 054063 (2020).
[10] C.-F. Li, G.-C. Guo, and J. Wang, Rep. Prog. Phys. **86**, 076001 (2023).
[11] L.-G. Wang, Z.-Y. Ou, and Y. Zhang, Adv. Quantum Technol. **5**, 2100123 (2022).
[12] N. Spagnolo et al., Nat. Commun. **4**, 1606 (2013).
[13] S. Chang, W. Ye, L. Hu, H. Zhang, and Z. Zhang, Phys. Rev. A **106**, 062409 (2022).
[14] I. Kogias, A. R. Lee, S. Ragy, and G. Adesso, Phys. Rev. Lett. **114**, 060403 (2015).
[15] X. Yu, Q. He, M. Reid, and P. D. Drummond, Phys. Rev. A **95**, 010101(R) (2017).
[16] Y. Zhang et al., Phys. Rev. Lett. **132**, 120401 (2024).
[17] R. Simon, Phys. Rev. Lett. **84**, 2726 (2000).
[18] G. Adesso, A. Serafini, and F. Illuminati, Phys. Rev. A **73**, 032345 (2006).
[19] X.-W. Liu, M.-H. Wang, and Q. He, Quantum Sci. Technol. **8**, 035005 (2023).
[20] A. Kumar, R. Ghosh, and S. L. Braunstein, J. Phys. A: Math. Theor. **55**, 305301 (2022).
[21] J.-Y. Chen, H. Zhang, and F. Xu, Phys. Rev. A **103**, 052412 (2021).